Z. Phys. D 40, 503–508 (1997)

ZEITSCHRIFT
FÜR PHYSIK D

Structural evolution of larger gold clusters

Charles L. Cleveland[1], **Uzi Landman**[1], **Marat N. Shafigullin**[2], **Peter W. Stephens**[3], **Robert L. Whetten**[2]

[1] School of Physics & Center for Computational Materials Science, Georgia Institute of Technology, Atlanta, GA 30332-0430, USA
[2] Schools of Physics & Chemistry, and Microelectronics, Research Center, Georgia Institute of Technology, Atlanta, GA 30332-0430, USA
[3] Department of Physics, State University of New York, Stony Brook, NY 11794, USA

Received 4 July 1996 / Final version: 5 September 1996

Abstract. The preferred structures of larger gold clusters comprised of 100 to 1000 atoms (1.4–3.0 nm equivalent diameter) have been determined theoretically via exhaustive search and energy-minimization methods and experimentally by synchrotron x-ray diffraction analysis of purified powder samples of small gold nanocrystals passivated by alkylthiol(ate) self-assembled monolayers. Theory predicts a persistent, close competition, across the entire size-range, among three structure-types: Marks-type decahedral (*Dh*) structures, monocrystals of a particular (*TO*+) truncated-octahedral (or 'Wulff') morphology, and symmetrically twin-faulted variants (*t-TO*+) of the second; all other forms are much less stable. Quantitative comparison of the experimental diffraction patterns with patterns calculated from the structures provides clear evidence for a high abundance of the *Dh* and *t-TO*+ forms, but also reveals a definite transition from the former to the latter structures in the 1.7 to 2.0 *nm* range ($\sim$ 200 atoms). Further, the observed (mean) lattice contraction is only about half that predicted, suggesting that the surfactant monolayer acts to reduce the surface energy of the clusters. Taken together, these results suggest that the surfactant monolayer may play a small but important role in differentially stabilizing the higher energy $\{100\}$-type facets present to a greater extent in the *TO*-type structures.

PACS: 36.40.Mr

I Introduction and Background

The size-evolution of the structures and structural transitions of larger clusters and *nm*-scale crystallites lies very near the heart of the broad fields of inquiry into these physicochemical systems. No element has been more instrumental than gold in stimulating the development of the main questions, whether in the unexpected discovery of noncrystallographic structure types (multiply twinned particles (MTPs): icosahedra, and the so-called Ino and Marks decahedra), or structural transitions (shape fluctuations, quasimelting, melting), all intertwined with the rise of high-resolution electron microscopy (HREM) as an unparalled investigative and visualizational tool. The richness of the diverse structures actually observed has posed an obvious challenge to systematic understanding, and, in spite of considerable effort over two decades, a consensus remains elusive. In an incisive and comprehensive recent review [1], Marks has critically assessed the following generalities:

(*i*) The vast majority of HREM-structural observations are on unannealed and hence metastable structures, from which false conclusions about equilibrium forms have been deduced, (notably the competitiveness of the MTP forms of larger nanocrystals);

(*ii*) The tendency of the act of observation itself (electron scattering) to change the cluster temperature, and thereby induce transformations;

(*iii*) The uncertain role, particularly at the smaller sizes ($< 10^3$ atoms), played by the completeness of the outermost structural shell, i.e. the "magic numbers" question, along with the associated questions of the stabilizing interaction with the support or with a ligand or surfactant shell, if present.

The most recent contributions to this issue have focussed, accordingly, at the large-cluster/small-particle boundary, from N $\sim$ 40 to $\sim 10^3$ atoms, or an equivalent diameter of $\sim$ 1.0 to 3.0 *nm*, with the following consequences:

(*i*) For ligand-free gold clusters imaged by HREM on supports, there is a basic conflict between results obtained using gas-phase annealing and softlanding methods, which produce monocrystalline structures of the truncated-octahedral (*TO* or "Wulff") form [2], and those obtained by annealing clusters aggregated on the support, which show that the thermally stable forms are decahedral (*Dh*) [3].

(*ii*) For preparative-scale gold clusters passivated by ligands or surfactant, evidence obtained by HREM has usually not been supported by comparison of powder x-ray diffraction patterns to structural models; the comprehensive analyses of Vogel and coworkers establish [4, 5] that the so-called Schmid Au_{55} cluster samples are mixtures of icosahedral clusters rather than the monocrystal cuboctahedral (*CO*) form deduced from HREM [6], and that the "hydrosol" *Au* cluster sample sized by HREM at 1.5 *nm* is better described as predominantly a *Dh* cluster of 2.2 *nm* diameter [7]. Not to be forgotten here is the largest cluster of any single element to be purified as a molecular compound and have its

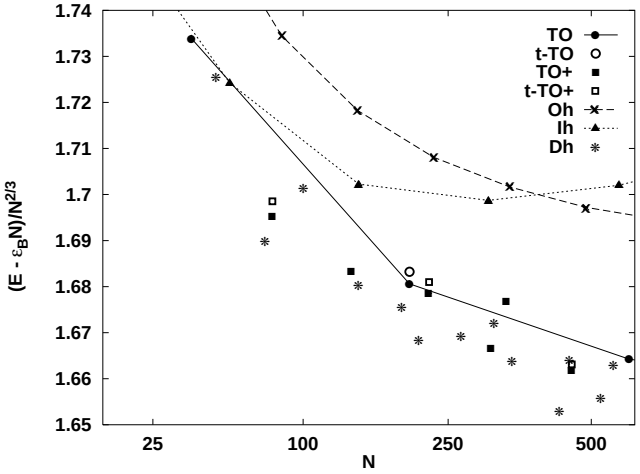

Fig. 1. Computed energies for certain fully relaxed Au_N structures, selected as described within from a large number considered, plotted vs. cluster size on a $N^{1/3}$ scale. The quantity ε_B = 3.93 *eV* is the cohesive energy per atom of bulk *fcc -Au*. See text for a description of these results and the symbols used

structure determined by rigorous x-ray crystallography, the *hcp* Au_{39} compound. [8] Somehwere in all other cases lurk the questions of purification and magic numbers.

(*iii*) From the theoretical side, the thorough analysis of structural energetics and strain based on continuum mechanical models provides considerable general insight, but must ultimately break down for a structure so small that a facet edge may contain only a small (integer) number of atoms [1, 9]. One requires an exhaustive search of atomistic structures, such as the one carried out for *Ni* clusters, [9] which has only recently been begun [10]. Its continuation is one of the main components of the present report.

Our approach involves three steps: first, the search for and exhaustive classification of the most stable (surfactant-free) Au_N clusters in the N = 40 to 1000 atom range; second, obtaining high-quality powder x-ray diffraction patterns for various samples of purified gold nanocrystals passivated by self-assembled monolayers (SAMs) of alkylthiol(ate) surfactant groups; third, quantitative comparison of the experimental patterns with those computed from the theoretical structures. In Sects. II to IV we describe these methods and give examples of the results. In Sect. V, we discuss an interpretation and reconciliation of the results by further invoking the wealth of knowledge pertaining to the *Au*/thiol SAM system.

II Theoretical prediction of stable forms

An exhaustive theoretical search for very stable Au_N clusters has led to the identification of three series or types of structures that are clearly superior to all others, including several (icosahedral, cuboctahedral) that have been seriously discussed as observed or preferred structures. As described in our earlier work [9, 10], the best available (embedded-atom) empirical potentials have been used, a very large group of unrelaxed structures have been constructed, and these are then relaxed to find the minimum-energy configuration. When plotted as a function of N, the cohesive energies of these particularly stable clusters form a band in Fig. 1 lying just below the solid line connecting the energies of the clusters of truncated-octahedral (*TO*) morphology (N = 38, 201, 586, . . .), which have the lowest energies of any of the regular or semi-regular archemidean polyhedral forms. [This form is sometimes referred to as the Wulff form, because for *fcc* lattices of atoms interacting via short-range pair-potentials it is the equilibrium morphology[9]] Also shown for reference are two other high-symmetry series (with connecting lines), the (Mackay) icosahedral (*Ih*) structures and the octahedral (*Oh*) structures. No other regular or semi-regular polyhedral series includes clusters that would appear on this diagram; in particular, members of the cuboctahedral series all have energies above 1.8 *eV* on this scale. The cohesive energies are plotted relative to the bulk *fcc* lattice energy of -3.93 *eV* per atom, and are divided by $N^{2/3}$ to normalize for surface area within any given series, so that a horizontal straight line will be obtained if the effects of facet boundaries (edge energies) and strain are negligible. We now describe separately the three competing series:

(*i*) Structures of the Marks-decahedral *Dh* type (see examples in Fig. 2) make up a large class of the very stable structures found. They are classified as multiply-twinned structures, although they are very nearly strain-free (cf. the *Ih* curve with its much larger volumetric strain), largely because of the notches (re-entrant facets) cut into the edges of the pentagonal prism portion of the structure. [The notch-free structures are known as Ino decahedra, and were found to be much less stable.] Among the very large number of structures falling under this description, the energetically competitive ones have a general shape (oblate, modest notch depth) that can be deduced by examining the three *Dh* structures shown in Fig. 2 (at N = 146, 212, 454) which are locally the most stable structures in Fig. 1.

(*ii*) Monocrystal structures of the TO+ type have been described fully in [10]. They are of course closely related to the ideal *TO* form, but have relatively larger $\{111\}$ and smaller $\{100\}$ facets, and so appear closer to the *Oh* form. They are generally as close to the true Wulff form as permitted by the constraint of integer numbers of lattice planes, until the $\{110\}$ truncation becomes possible at $\sim 10^4$ atoms. Structures of the *TO*++ type and *TO*- type, representing greater and lesser $\{111\}$ truncations of the cube, respectively, generally lie clearly higher in energy than the *TO* line (Fig. 1) for $N < 1000$, and are omitted from the diagram for reasons of clarity.

(*iii*) Symmetrically twinned structures (*t-TO*+) derived from certain of the *TO*+ clusters are also described in [10], and two examples are presented in Fig. 2b,c. The point-group symmetry is lowered from cubic to D_{3h} symmetry, with the threefold axes lying perpendicular to the twinning plane, and three large, gradually re-entrant regions are created about the symmetry axis. These lie only very slightly higher in energy than their monocrystalline variants, reflecting the generally near-vanishing internal energy of a stacking fault (in *fcc* -metals) and the special result for these symmetric clusters that the surface energy is negligibly affected by twinning.

In every case, the structures have been relaxed fully, a process that results in an overall (radial) contraction of 2-3% (relative to bulk *fcc* gold) that is slightly stronger at the vertices and edges, resulting in structures that appear more rounded (less faceted) than the polyhedral names would sug-

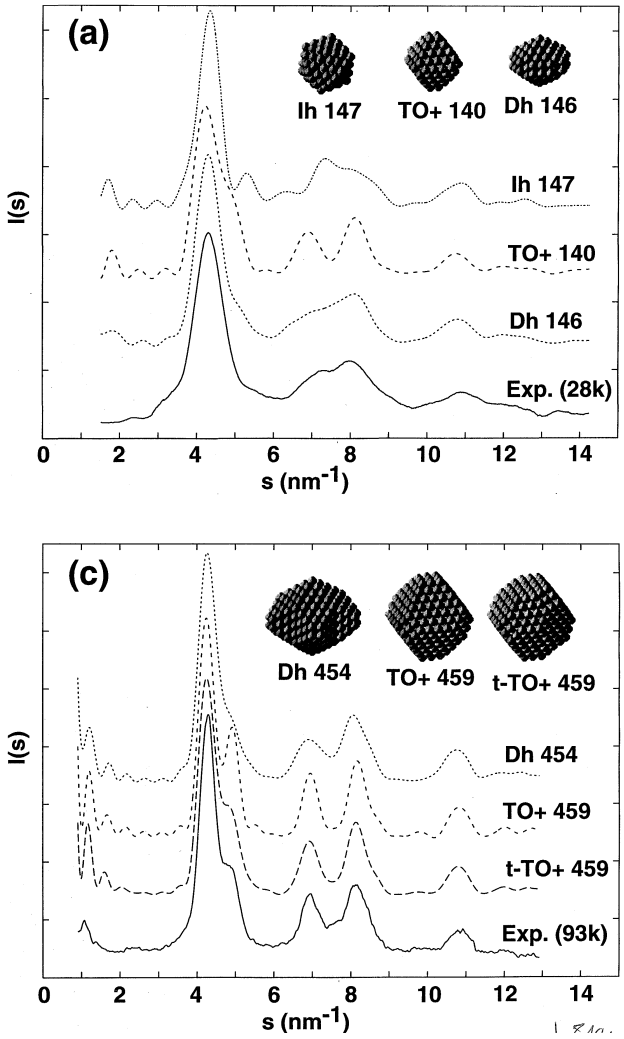

Fig. 2a–c. Examples of experimental diffraction patterns (below, labelled "Exp." followed by the mass of the cluster) and diffraction patterns calculated from fully relaxed Au_N structures (inset in each frame). The diffraction patterns in each case are displaced along the vertical axis for clarity of exposition. **a** Diffraction pattern for a powder sample of 28*k Au* on a silicon substrate, obtained in reflection. **b** Diffraction pattern for a sample of 45*k Au* on a mica substrate, obtained in transmission. **c** Diffraction pattern for a film sample of 93*k Au* on mica, obtained in transmission. [The re-entrant (Marks' decahedral) structures are classifed, using the notation established in [9], as follows: **a** *Dh*-146 is (3,2,2); **b** *Dh*-212 is (2,2,3); and **c** *Dh*-454 is (2,2,4). See text for a description of the selection of these structures, along with a full description of the comparisons and other notations]

gest. We describe in Sect. IV how these structures are used in comparison with x-ray diffraction patterns of *Au* clusters passivated by a surfactant monolayer.

III Synchrotron x-ray diffraction from samples of nanocrystal gold molecules

Examples of x-ray diffraction (XRD) patterns obtained on samples of nanocrystal gold molecules are shown in Fig. 2. These are purified fractions of materials prepared and separated by methods described in [10], and each has undergone a separate characterization involving also small-angle x-ray diffraction and mass spectrometry. They will be referred to by their core masses, (a) 28*k*, (b) 45*k*, and (c) 93*k*, where k = 10^3 atomic mass units (~ 5 *Au* atoms). The lighter two fractions, Fig. 2(a,b), are obtained from samples where the surfactant used is dihexyldisulfide, giving rise to a short-chain monolayer hereafter referred to as C_6S [11]. Their core-diameter equivalents, as calculated from mass spectrometry, are 1.7 ± 0.1 *nm* and 1.9 ± 0.2 *nm*, respectively, corresponding to Au_N aggregation numbers of $N = 140$ and 220 atoms with uncertainties of about 10 atoms and 20 atoms, respectively. The heavier fraction shown is a sample prepared from dodecylthiol, hereafter $C_{12}S$, which has a core diameter near 2.5 ± 0.2 *nm*, or $N = 460 \pm 30$ atoms. A further sample of the same core-mass but with C_6S surfactant gives an essentially superimposable XRD pattern, showing that the pattern is independent of the chain-length. Because these samples have been highly purified, we believe that the uncertainties quoted represent limitations of the size-measuring method, rather than actual spreads in cluster size; the analysis and interpretation of the results given below is consistent with, but does not necessarily prove, this hypothesis.

The XRD patterns shown are obtained in the $(\theta,2\theta)$ configuration on powder (*a*,*b*) or film (*c*) samples prepared on either a miscut Si (111) wafer for reflection (*a*) or on extremely thin mica plates for transmission (*b*,*c*) measurements, using synchrotron radiation ($\lambda = 0.115$ *nm*) at the X3A beamline of the National Synchrotron Light Source at Brookhaven National Laboratory. The samples all show good crystallinity (correlation lengths of 30 to 100 times the superlattice constant) in the small-angle (superlattice) diffraction region, a further indication of sample purity. We have also verified for the 93*k* sample (*c*) that the essential features of the pattern are not altered when a powder sample is used instead.

In every case, the main features in the powder patterns in Fig. 2 can be indexed to *fcc -Au*, with a slight contraction in the lattice constant, and the widths of the peaks can be

ascribed loosely to the finite-size of the crystallites, using the standard approximate equations. Further, a preliminary assessment can be formed as to the likely structural characteristics by comparing the features of the pattern to those of published calculations. However, such approximations and "pattern-recognition" exercises fail completely to account for the specific lineshapes observed and even for the relative intensities of the peaks. To account for all this rigorous and sample-specific information, one must perform direct calculations or simulations of the structure factors based on atomistically detailed structures, as described in the next section.

IV Comparison of experimental and calculated XRD patterns

Diffraction patterns, such as those displayed in the upper portions of Fig. 2a–c, are calculated from the structures obtained as described in Sect. II, using the Debye formula [12], which describes the diffraction from an ensemble of identical objects that are spatially and orientationally uncorrelated. [The absence of discernable fine-structure on the experimental lineshapes constitutes prima facie evidence against significant correlations.] Each object consists of *N* atoms located according to the structural model, from which one calculates the diffracted intensity *I*(*s*) as a function of the diffraction vector length $s = \frac{2\sin\theta}{\lambda}$ as

$$I(s) = \sum_{i,j=1}^{N} f_i f_j \frac{\sin(2\pi s x_{ij})}{2\pi s x_{ij}}$$

where x_{ij} is the distance between *i*th and *j*th atoms in the cluster and (f_i, f_j) are their corresponding atomic scattering factors. The comparison to experimental XRD patterns involves several additional steps. The contribution of scattering from the support is measured independently and subtracted. The calculated scattering function is then multiplied by angular dependent geometry and polarization factors, expressed in composite form as $\frac{cos\theta}{(1+\alpha cos^2 2\theta)}$, where α depends on the polarization of the incident x-rays. For unpolarized radiation α is equal to unity, while it vanishes for instruments (as here) which employ radiation highly polarized perpendicular to the plane of incidence. To account for thermal effects, a damping factor $\exp(-\frac{Bs^2}{2})$ is applied to the calculated intensity. The value of *B* is determined by a routine which employs nonlinear least-squares fit to achieve the best agreement between theory and experiment. [If the obtained *B*-value does not vanish at low temperatures, then it is supposed to reflect also a kind of static random disorder (or strain).] Two further parameters are found to be necessary in order to obtain consistent comparisons: the background (or zero-signal level) is allowed to vary linearly with *s*, and a scaling factor generates a uniform expansion or contraction of the cluster.

In each of the frames of Fig. 2, an experimental XRD pattern is displayed on the same scale as *I(s)* patterns calculated from three directly relevant structures, where *B* and the uniform scaling parameter have been varied to obtain the best fit to experiment. Although fully quantitative assessments of the goodness of the fits (chi-squared values) are available for these (and for other calculated) structures, the results are so decisive that a direct visual inspection of the patterns is sufficient. We therefore proceed to describe these in the order they are shown:

(*a*) The 28*k-Au* experimental pattern has a lineshape whose essential features are all captured by the *Dh*-146 cluster and not by any of the monocrystalline or icosahedral forms in the same size-range. [In the comparison shown, the values B = 0.013 nm^2 and an uniform-expansion factor of 1.033 have been applied to the calculated *I(s)*.] In particular, the experimental lineshape in the s = 4 to 10 nm^{-1} range is captured extremely well by this structure, with the exception that the experimental pattern exhibits what appears to be an elevated background in the 5 to 6 nm^{-1} region. We believe that this can be attributed to diffuse scattering from the hydrocarbon (*C-C*) chains of the surfactant groups, which are relatively more significant in the smallest clusters. The monocrystalline form is clearly ruled out on the basis of the profile of the (111,200) peak complex as well as the clear separation of the (222) and (311) peaks; introduction of a stacking fault (or twinning) of this structure also fails by comparison of the (222)-(311) region. A nonrigorous comparison with hcp-type powder patterns also fails to produce a satisfactory starting point for explanation of the experimental structure. On the other hand, *any* of the *Dh*-type structures constructed and relaxed in the N = 127 - 156 region provide a better explanation, and we show *Dh*-146 not because it is clearly the best but because it is inherently more plausible on energetic grounds (Fig. 1) than are the others. A further refinement of the experimental background issue is necessary before a decision can be made among the *Dh* structures. As a point of comparison, Vogel et al [5]. obtained a good fit for the nominal 1.5-*nm Au* hydrosol (unpurified) XRD pattern only by using a ∼20:80 weighting of two very different decahedral structures (with N = 181 and 428 atoms, respectively).

(*b*) The 45*k-Au* experimental pattern has a lineshape whose essential features are all captured by the *t-TO*+ 225 cluster and not by any of the monocrystalline or multiply-twinned forms in the same size-range. [The comparison shown uses the values B = 0.010 nm^2 and a uniform-expansion factor of 1.014.] In particular, the experimental lineshape of the (111,200) peak complex (s = 4 to 6 nm^{-1}) range is captured extremely well by this structure. [The sharp weak features are diffraction from the thin mica substrate.] The monocrystal variant of this structure (*TO*+ 225) notably fails to capture the degradation of the (200) and (400) peaks, among other deficiencies, while the decahedral *Dh*-212 structure is too broad throughout.

(*c*) The 93*k-Au* experimental pattern has a lineshape whose essential features are also all captured by a symetrically twinned structure, *t-TO*+ 459, and not by any monocrystalline or multiply-twinned forms in the same size-range. [The comparison shown uses the values B = 0.017 nm^2 and a uniform-expansion factor of 1.014.] A preliminary description of this comparison has been given in [10], including a plotted residual showing the high level of agreement throughout; a full report on the comparison to other twinned structures and incorporating structural information from the small-angle diffraction from an ordered superlattice, will be presented elsewhere. The deficiencies of the monocrystalline

and decahedral forms in capturing the essentials of the experimental pattern follow closely those described above for 45*k-Au*, and so are not repeated here.

We have further obtained large-angle XRD patterns for many other fractions, mostly using conventional rather than synchrotron radiation, and made cursory comparisons with patterns calculated from a multitude of structures. These results confirm that samples of core mass above 40*k* (and extending to 140*k*) are all twin-faulted *fcc* , whereas those below 40*k* are decahedral, or even icosahedral (near or below 20*k*).

A feature common to all the refinements is that the theoretical structure needed to be slightly enlarged using a scaling factor in the 1.01 to 1.03 range. Considering that the theoretical structures show a mean contraction from the bulk structure of two to four percent in this size-range, one concludes that the passivated gold clusters undergo only about half of the contraction expected. The implications of this robust conclusion are discussed in the next section.

We emphasize here that the procedure used to obtain the comparisons produced in Fig. 2a–c are in no sense a kind of free-form "refinement" in which atoms (or groups of atoms) are allowed to move relative to each other; only a single scaling parameter is adjusted, and its value lies well within the physically plausible range. There is no question that a free-form refinement starting from the "best" structures would result in an improved fit, but only at the risk of leaving the realm of physical plausibility established by use of accurate, tested empirical potentials.

V Reconciliation of the evidence

It is satisfying that one is able to account for the experimental patterns using structures from the three classes of very stable structures found by exhaustive search and energy-minimization methods, while at the same time eliminating so many other structural classes. However, there are several issues that point toward a more refined interpretation. First, the theory predicts that *Dh*-type clusters should remain energetically competitive to larger sizes, to 3 *nm* or larger, in agreement with the annealing-based HREM investigations of surfactant-free gold clusters, [3] whereas the XRD and HREM evidence [10, 13, 14] on gold nanocrystals passivated by alkylthiol monolayers are quite convincing that a definite transition to *fcc* (monocrystal and singly twinned) forms takes place, probably at no greater than $\sim$ 1.8 *nm* (180$\pm$ 30 atoms). Second, the deviation from the predicted magnitude of the lattice contraction suggests that improvements are needed in the description of the surface energies. Third, the evidence that twinning is heavily preferred, even though the energy cost is expected to be zero or slightly positive, is interesting. Such twins may result from residual stresses accumulated during the growth of the cluster; that is, they may be "annealing twins," as described in the physical metallurgy literature [15].

Our purpose here is to point out that a great deal of relevant information is available on the packing and energetics of the alkylthiol(ate) monolayers on gold, particularly from the recent simulations [16], and generally because these are the nanocrystal analogs of the exceedingly popular noble-metal thiolate self-assembled monolayer (SAM) surface systems.[17] The properties of such $Au_N(SR)_M$ assemblies, and for planar surfaces, include that the surfactant head-groups form a compactly packed mantle surrounding the core, with ratios of *S* to surface *Au* atoms in the range of 1:2 to 1:3, depending on the exposed facet, but somewhat higher in 1.5 - 2.5 *nm* diameter nanocrystals; and that the adsorption (desorption) energy [18] of $\sim$ 1.3 *eV* per dimeric *RS-SR* molecule (dialkyldisulfide) adsorbed thus is small ($<$ 0.3 *eV* per surface *Au* atom) compared to the cohesion of *Au* (3.9 *eV* per atom) and comparable to the unusually low surface energy of Au ($\sim$0.4 *eV* per surface atom), consistent with minimal disruption of the gold surface structure and a probable *S-Au* bonding mode involving only the nonbonding electrons of an intact *RSSR* molecule [19]. Although this reduction in the surface energy is relatively small, it does point to one clear mechanism by which the lattice contraction is reduced. Further, since this surface energy lowering is facet-type dependent, it reduces the cost of (100) facets more than that of (111) facets, its net effect may be an earlier than expected stabilization of the single-crystal forms, including their twins.

The assistance of I. Vezmar (MS analysis), J.T. Khoury (preparation and separation) is gratefully acknowledged. Financial support has been provided by the Georgia Tech Research Foundation, the Packard Foundation and the Office of Naval Research (to RLW), and the U.S. Department of Energy and the Air Force Office of Scientific Research (CC and UL). Calculations were performed on CRAY computers at the National Energy Research Supercomputer Center, Livermore, California, and at the GIT Center for Computational Materials Science. Research carried out in part at the National Synchrotoron Light Source, Brookhaven National Laboratory, which is supported by the US Department of Energy, Division of Materials Sciences and Division of Chemical Sciences. The SUNY beamline at NSLS is supported by the Division of Basic Energy Sciences of the US Department of Energy (DE-FG02-86ER45231).

References

1. For a comprehensive review, see L. D. Marks, Rep. Prog. Phys. **57**, 603-649 (1994)
2. A. N. Patil, D. Y. Paithankar, N. Otsuka, R. P. Andres, Z. Phys. **D26**, 135 (1993)
3. L. D. Marks, private communication to one of the authors (RLW)
4. W. Vogel, B. Rosner, B. Tesche, J. Phys. Chem. **97**, 11611-11616 (1993)
5. W. Vogel, D. G. Duff, A. Baiker, Langmuir **11**, 401-404 (1995)
6. L. R. Wallenberg, J. O. Bovin, G. Schmid, Surf. Sci. **156**, 256 (1985)
7. D. G. Duff, A. Baiker, P. P. Edwards, J. Chem. Soc. Chem. Commun. 1993, **97** (1993); Langmuir **9**, 2301 (1993)
8. B. K. Teo, X. Shi, H. Zhang, J. Am. Chem. Soc. **113**, 2743 (1992)
9. C. L. Cleveland, U. Landman, J. Chem. Phys. **94**, 7376 (1991)
10. R. L. Whetten, J. T. Khoury, M. M. Alvarez, Srihari Murthy, I. Vezmar, Z. L. Wang, P. W. Stephens, C. L. Cleveland, W. D. Luedtke, U. Landman, Adv. Mater. **5**, 428-433 (1996); R. L. Whetten, J. T. Khoury, M. M. Alvarez, S. Murthy, I. Vezmar, Z. L. Wang, C. L. Cleveland, W. D. Luedtke, U. Landman, in "Chemical Physics of Fullerenes 5 and 10 Years Later", pp. 475-490. W. Andreoni (ed.) Dordrecht: Kluwer 1996
11. M. Shafigullin, I. Vezmar, J. T. Khoury, R. L. Whetten (submitted)
12. A. Guinier, "X-Ray Difraction". San Francisco: Freeman 1963
13. M. Brust, M. Walker, D. Bethell, D. J. Schiffrin, R. Whyman, J. Chem. Soc. Chem. Commun. **801** (1994)
14. Z. L. Wang, unpublished HREM observations

15. G. E. Dieter, Mechanical Metallurgy, pp. 104-107. New York: McGraw -Hill 1961
16. W. D. Luedtke, U. Landman, J. Phys. Chem. **100**, 13323 (1996)
17. L. H. Dubois, R. G. Nuzzo, Annu. Rev. Phys. Chem. **43**, 437 (1992)
18. R. G. Nuzzo, B. R. Zegarski, L. H. Dubois, J. Am. Chem. Soc. **109**, 733-740 (1987); see also C. D. Bain, E. B. Troughton, Y.-T. Tao, J. Evall, G. M. Whitesides, R. G. Nuzzo, J. Am. Chem. Soc. **111**, 321 (1989)
19. P. Fenter, A. Eberhardt, P. Eisenberger, Science **266**, 1216 (1994)